Bulletin of the Seismological Society of America, Vol. 108, No. 3B, pp. 1683–1694, July 2018, doi: 10.1785/0120170248

Geomorphological Influences on the Distribution of Liquefaction in the Wairau Plains, New Zealand, Following the 2016 Kaikōura Earthquake

by Sarah H. Bastin, Matt Ogden, Liam M. Wotherspoon, Sjoerd van Ballegooy, Russell A. Green, and Mark Stringer

Abstract The 2016 M_w 7.8 Kaikōura earthquake triggered localized liquefaction and associated lateral spreading in the Wairau Plains on the South Island of New Zealand. Detailed postevent mapping from ground and helicopter-based reconnaissance indicates that liquefaction predominantly manifested proximal to rivers and streams within the easternmost extent of the plains. In this study, pre- and postevent light detection and ranging (lidar) survey data and aerial photography are analyzed to further resolve maximum extents of liquefaction-induced damage and to infer the presence and/or absence of liquefaction in areas that were not covered during reconnaissance surveys. Historical maps used in conjunction with local geomorphologic and topographic variability are shown to provide insights into the depositional settings of areas where liquefaction manifestations were observed. Cone penetration test (CPT) logs are additionally utilized to examine characteristics of the subsurface soil profiles in areas where liquefaction did and did not manifest. The various data sources indicate that the observed distributions of liquefaction manifestations within the lower Wairau Plains correlate with basic depositional processes of meandering rivers and correspond with the position of point-bar and paleochannel deposits. This study highlights the potential applications and benefits of incorporating geomorphic and topographic variability into liquefaction hazard assessments.

Introduction

Liquefaction and associated phenomena (e.g., lateral spreading) pose a significant hazard to the built environment, as observed following many recent and historical earthquakes (e.g., Quigley *et al.*, 2016; Geotechnical Extreme Event Reconnaissance [GEER], 2017). Liquefaction-induced land damage has also been attributed to increased secondary hazards, such as flooding (e.g., Hughes *et al.*, 2015). The direct and secondary hazards posed by liquefaction highlight the need for local authorities to adequately assess liquefaction hazards and effectively manage the consequences to the built environment. Liquefaction hazard assessments may utilize the distribution of low-lying Quaternary-aged alluvial deposits from geological maps to determine likely distributions of sediments with low cyclic resistances to liquefaction. The hazard is further refined from geotechnical assessment of *in situ* testing (e.g., simplified cone penetration test [CPT]-based liquefaction triggering procedures). These site-specific assessments often rely solely on the results of the geotechnical *in situ* test-based procedures, with little to no consideration given to local geomorphology, historical maps, and/or historical distributions of liquefaction. Previous studies have shown that distributions of liquefaction manifestations following recent earthquakes typically correspond with the position of active and paleo-river channels, such as that highlighted following the 2010–2011 Canterbury earthquake sequence (CES; Wotherspoon *et al.*, 2012) and the 2011 Tohoku earthquake (Wakamatsu, 2012). These studies highlight the relationship between geomorphology and observed distributions of liquefaction manifestations and thus reiterate the benefit of incorporating detailed desktop studies into liquefaction hazard assessments. Recurrent liquefaction has also been documented at sites of liquefaction manifestation following the 2011 Tohoku earthquake, indicating that the underlying sediments remained highly susceptible to liquefaction (Wakamatsu, 2012). Detailed documentation of the distributions of liquefaction manifestations following recent events therefore enables the geomorphologic settings and soil profiles in areas where liquefaction typically does and does not manifest to be examined in detail.

The 2016 M_w 7.8 Kaikōura earthquake triggered localized liquefaction in the Wairau Plains on the South Island of New Zealand (GEER, 2017; Stringer *et al.*, 2017). A horizontal peak ground acceleration (PGA) of 0.22g was recorded at the MGCS strong-motion station in the lower reaches of the plains (GEER, 2017). Postevent reconnaissance mapping provided an overview of the distribution of

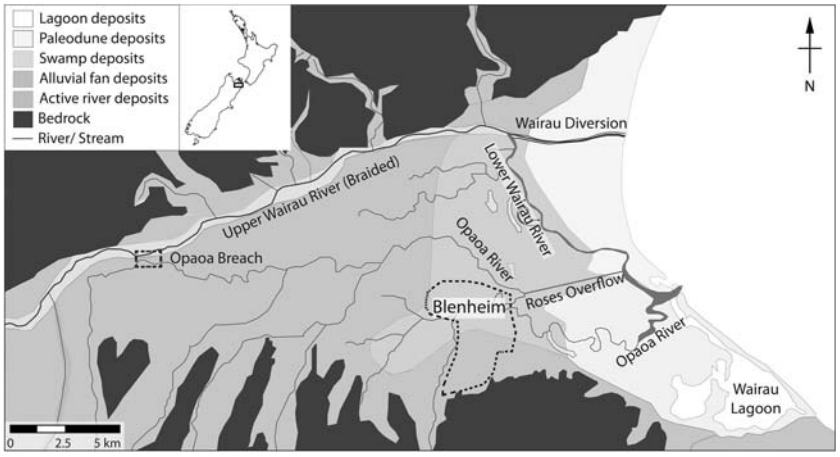

Figure 1. Near-surface sediments present in the Wairau Plains, with the position of rivers and streams indicated with respect to the township of Blenheim (dotted box). The location of the Ōpaoa Breach (dashed box) to the west of the township is also indicated.

liquefaction manifestations within the wider Wairau Plains area; however, this was limited to the areas covered during the ground and helicopter-based surveys (GEER, 2017). Initial mapping suggests that localized cases of lateral spreading and associated surface manifestations of liquefaction ejecta occurred proximal to rivers to the east of the township of Blenheim (indicated in Fig. 1; GEER, 2017; Stringer *et al.*, 2017). This article provides an overview of the distributions of liquefaction manifestations within the lower Wairau Plains following the 2016 Kaikōura earthquake, as derived from reconnaissance and remote sensing techniques. The influences of geomorphic and sedimentologic variability on the observed distribution of liquefaction-induced damage are subsequently discussed, with the goal of highlighting the importance of incorporating local geomorphic variability into liquefaction hazard maps and land-use planning decisions for local and regional authorities.

Geologic and Geomorphic Setting

The Wairau Plains are situated in the northeastern corner of the South Island of New Zealand (Fig. 1). The plains are bounded by northeast-trending mountain ranges reflecting uplift along the Wairau and Awatere faults. The faults comprise part of the Marlborough fault zone, a zone of northeast-trending transpressional faulting associated with the offshore transition of the plate boundary (Rattenbury *et al.*, 2006). Tectonic deformation combined with soft sediment compaction results in ~4.2 mm/yr of subsidence within the lower portion of the plains (Rattenbury *et al.*, 2006).

The Wairau Plains comprise the alluvial outwash plain of the Wairau River and are predominantly underlain by re-worked glacial outwash gravels, sands, and silts sourced from the surrounding mountains (Fig. 1; Basher *et al.*, 1995). The active floodplain of the Wairau River avulsed across the Wairau Plains prior to European settlement, as reflected by the many active and paleo-river channels that transect the surface of the plains. The Wairau River transitions from braided to meandering ~7 km inland from the coast as a result of decreasing topographic gradient (Fig. 1).

The township of Blenheim (population ~30, 700) is located ~5 km from the coast and upon the Wairau Plains (Fig. 1). Blenheim is predominantly underlain by Holocene-aged fluvial and swamp deposits composed of poorly consolidated sand, silt, and peat (Brown, 1981). Sediments were initially deposited during flood events of the Wairau River and have subsequently been re-worked by the meandering Ōpaoa (previously named Opawa) and Taylor Rivers that flow through the township (Fig. 2; Basher *et al.*, 1995). Low topographic relief in the vicinity of Blenheim combined with regular flooding resulted in large swamps forming within much of the area now occupied by Blenheim (Fig. 1; Basher *et al.*, 1995). Paleochannels and associated crevasse splay deposits are present across the lower portion of the plains and reflect channel avulsion and bank-overtopping flood events prior to settlement of the area. Sediments to the east of the township are interfingered with lagoonal muds and coastal sands, silts, and gravels associated with coastline progradation and marine regression following the mid-Holocene highstand at 6000 yrs before present (Fig. 1; Brown, 1981; Basher *et al.*, 1995). Gravel beach ridges are present from the modern coastline to 5.5 km inland, whereas discontinuous sand dunes are present from 5.5 to 7 km inland and reflect the position of the paleocoastlines (Fig. 1; Basher *et al.*, 1995). The course of the meandering section of the Wairau River is diverted around the beach ridges, which are of sufficient height and erosional resistance that the river has maintained its position for at least the last 2000 yrs (Christensen and Doscher, 2010).

Significant river control and drainage works have been undertaken within the lower portion of the Wairau Plains in an attempt to reduce flooding. Stopbanks (levees) were constructed along the banks of the meandering Taylor and Ōpaoa Rivers within central Blenheim as part of the initial drainage works (indicated in Fig. 2; Marlborough Catchment Board, 1959; Christensen and Doscher, 2010). The stopbanks were subsequently raised and moved back between 1921 and 1956, at which time the Taylor River was straightened within central Blenheim. Stopbanks were additionally constructed along the Upper Wairau River as part of flood-protection works to reduce overbank flows through Blenheim. A partial breach of the stopbank occurred during a flood in 1861, causing the Wairau River to partially divert into the Ōpaoa River (location shown in Fig. 1). The increased flow resulted in widening of the channel and led to significant flooding within Blenheim (indicated in Fig. 1; Marlborough Catch-

ment Board, 1959). The breach was not successfully re-blocked until 1917, at which point the flooding hazard was transferred downstream. Remedial works including straightening of an S-bend were subsequently undertaken to reduce flooding of the Lower Wairau River. Work culminated in the construction of a diversion channel that provides a direct route from the braided Upper Wairau River to the ocean (Christensen and Doscher, 2010). The unprotected floodplain surrounding the Lower Wairau and Ōpaoa Rivers is highly susceptible to flooding, with overbank flood events regularly depositing loosely consolidated fine sand to silt in these areas. Flooding in the distal floodplains protected by the stopbank network is limited to major events (i.e., 20–50 yr events; Christensen and Doscher, 2010).

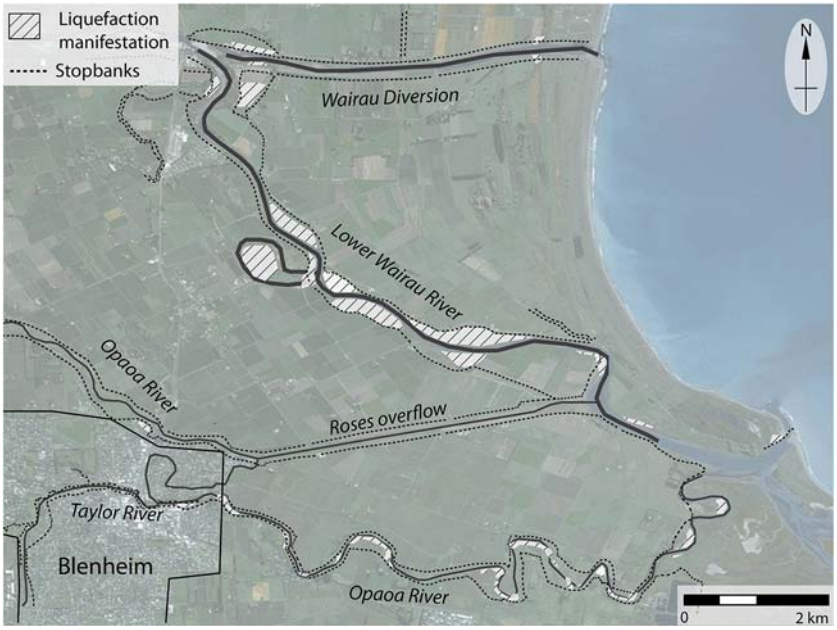

Figure 2. The distribution of liquefaction manifestations as mapped within the Wairau Plains through postevent ground and helicopter-based reconnaissance surveys following the 2016 Kaikōura earthquake. The position of the Wairau and Ōpaoa Rivers and associated stopbank network is indicated with respect to the Blenheim urban area (modified from Stringer *et al.*, 2017). The color version of this figure is available only in the electronic edition.

Methodology

Reconnaissance Mapping

The surficial manifestations of liquefaction were mapped in detail through ground-based reconnaissance investigations by researchers and practicing engineers between November and December 2016. Observed extents are shown in Figure 2, whereas field examples are shown in Figure 3. Observational records were supplemented with reports from local residents and mapping conducted by the local council and engineering firms (presented in Stringer *et al.*, 2017). Ground-based mapping was additionally supplemented with observations from high-resolution postevent aerial photography taken during helicopter reconnaissance of the stopbank network in the days following the event (Fig. 3). The use of ground-based surveys and postevent photography provides a comprehensive overview of the damage in areas severely affected by liquefaction and associated lateral spreading. The methodology however does not capture areas of marginal manifestation nor damage in areas not targeted during reconnaissance investigations.

Lidar-Derived Ground-Surface Subsidence

Extents of liquefaction manifestation may additionally be derived and further refined from analysis of measured vertical ground-surface displacements that likely represent settlement induced by lateral spreading, volumetric densification, and ejection of liquefied sediment. Vertical displacements were derived as part of this study from the comparison of pre- and postevent digital elevation models (DEMs) created from light detection and ranging (lidar) surveys and are shown in Figure 4. Pre-event lidar was flown in 2014 by the Marlborough District Council. The resultant DEM has a minimum spatial resolution of 2 m and a processed vertical accuracy of ± 0.06 m, which was derived from comparison of derived and field survey points. Postevent lidar was flown over the lower section of the Ōpaoa River in the month following the earthquake by AAM Ltd., as commissioned by Land Information New Zealand (LINZ). The DEM has a minimum resolution of 1 m and a processed vertical accuracy of ± 0.05 m. The height accuracy of the classified ground points from the lidar survey was cross checked by comparing field survey points with the calculated height-difference statistics between a Triangulated Irregular Network (TIN) of the lidar ground points. The postevent DEM was subtracted from the pre-event DEM to derive a differencing model. The resultant model has a minimum spatial resolution of 2 m and a vertical accuracy of approximately ± 0.1 m. Vertical displacements < 0.1 m are therefore inferred to be within the error range of the model and are omitted from further analysis. Benchmark surveys performed by LINZ indicate tectonic movements of the Kaikōura earthquake were on the order of 50 mm in the wider Wairau Plains. Tectonic displacements were removed from the dataset by determining a baseline difference between the pre- and post-DEMs that was subtracted during the differencing process. The resultant differencing model therefore represents local displacements (e.g., resulting from liquefaction).

It is acknowledged that there are additional methodologies by which vertical displacements may be derived. For example, work by Chini *et al.* (2015) utilized Differential Interferometric Synthetic Aperture Radar (DInSAR) from high-resolution pre- and postevent satellite imagery to map

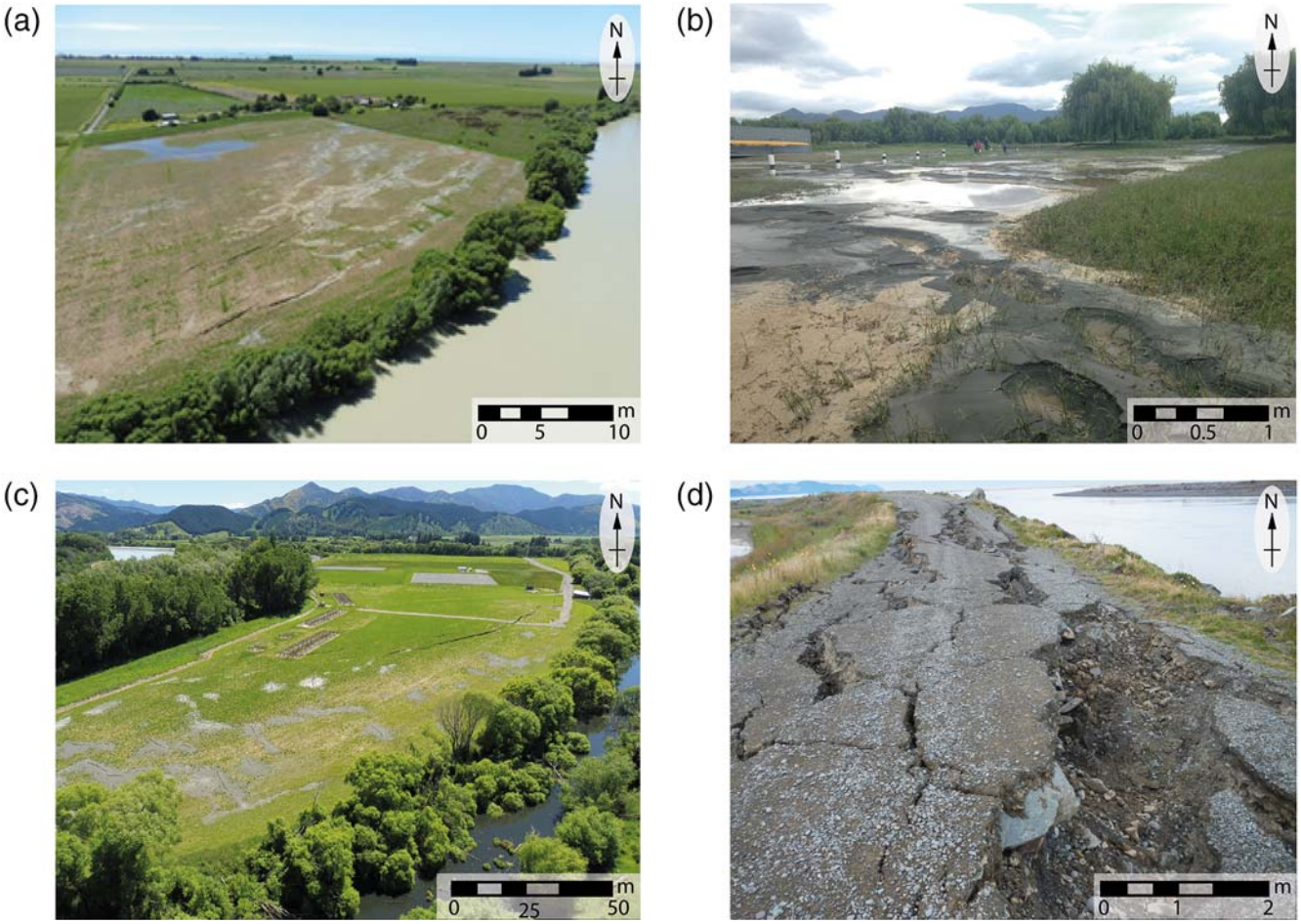

Figure 3. (a) Aerial photographs from helicopter-based reconnaissance illustrating liquefaction-induced damage along the Lower Wairau River. Lateral spreading-induced cracking is observed proximal to the river bank and transitions into lineaments of aligned sand boils distal to the river bank. (b) Example of surface manifestations of liquefaction ejecta, as observed at the Blenheim Rowing Club during ground-based reconnaissance. (c) Surface manifestations of lateral spreading observed at the Marlborough Equestrian Centre from helicopter-based reconnaissance. Features appear to align with the former channel of the Wairau River in the foreground; the current channel of the Wairau River is visible in the background. (d) Example of a stopbank failure as observed along the Wairau Diversion during ground-based reconnaissance. The color version of this figure is available only in the electronic edition.

liquefaction effects and vertical displacements with an error range of < 1 cm. DInSAR was not applied in this study because the processed data were not available at the time of analysis. In addition, the methodology of deriving vertical ground displacements from lidar had previously been applied by the researchers of this study following the 2010–2011 CES (i.e., Tonkin and Taylor, 2015) and thus enabled direct comparison of the application of this technique and the resultant error ranges.

Deriving Horizontal Ground-Surface Displacements from Comparison of Pre- and Postevent Aerial Photography

Comparison of the horizontal position of objects identified within pre- and postevent aerial photography provides a methodology by which horizontal ground-surface displacements may be derived. Horizontal ground-surface displacements indicate areas affected by lateral-spreading-induced ground-surface displacements and provide an indication of the magnitude and directionality of the displacements. Vectors outlining the directions and magnitudes of horizontal movement were derived as part of this study from comparison of the horizontal position of objects in the pre- and postevent aerial photography and are presented in Figure 4. Pre-event aerial photography was flown in 2015–2016 by AAM for LINZ; postevent aerial photography was flown shortly after the event by AAM for LINZ. Both datasets have a 2-m spatial resolution. The horizontal position of 200 randomly spaced features including buildings, road markings, and fence corners were manually digitized within the pre- and postevent imagery in areas where lateral spreading was and was not reported. Features affected by tilt in the imagery and/or anthropogenic modification were identified during manual selection and omitted from further analysis. The horizontal position of objects identified in the pre- and postevent imagery was subsequently compared, and vectors outlining the horizontal

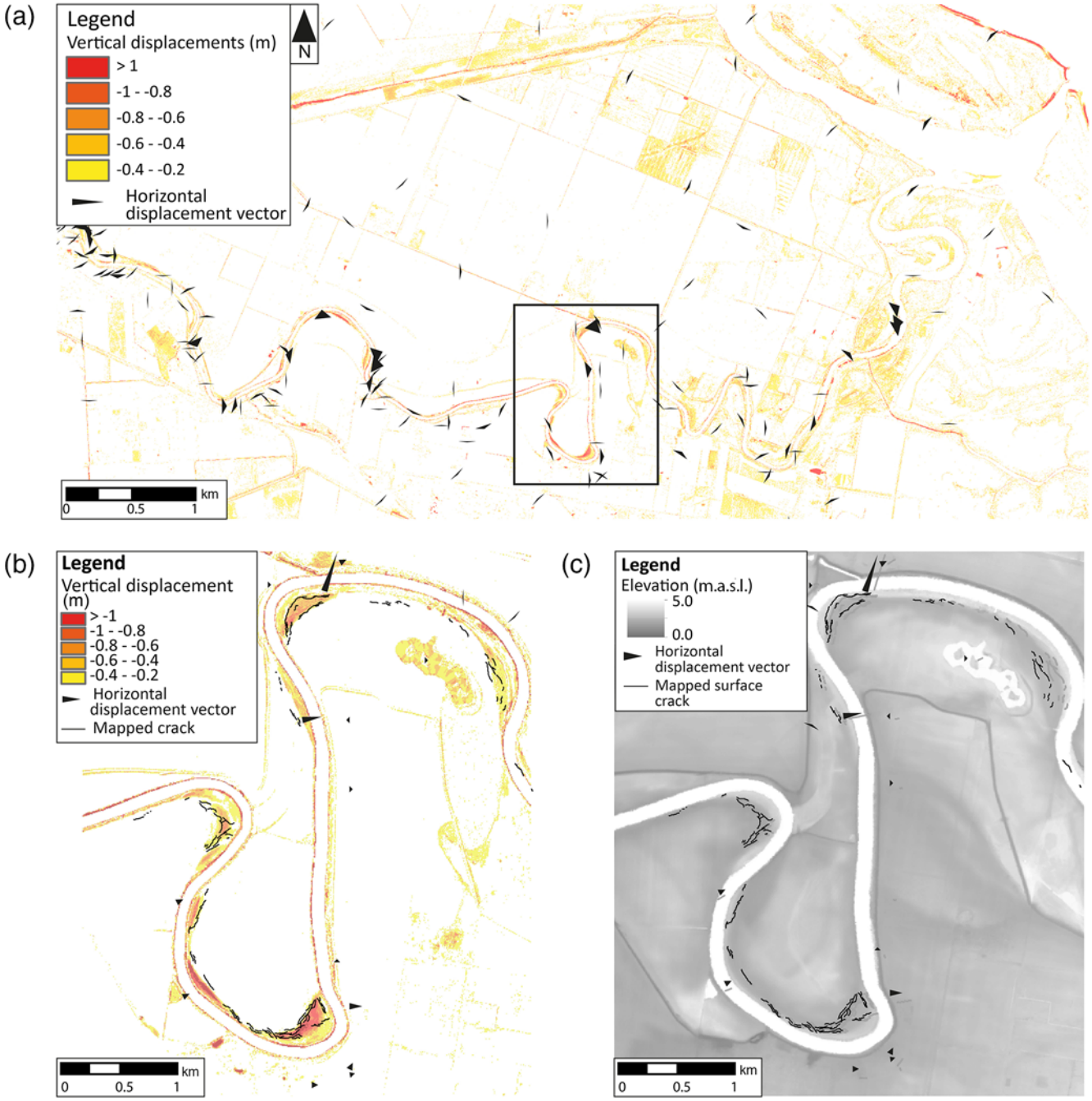

Figure 4. (a) Vertical ground displacements as derived for the Ōpaoa River from comparison of pre- and postevent light detection and ranging (lidar) surveys overlain with horizontal displacement vectors created from pre- and postevent aerial imagery. Box indicates the area shown in (b) and (c). (b) Horizontal and vertical ground displacements derived for the area following the Kaikōura earthquake overlain with ground-surface cracks mapped from postevent helicopter- and ground-based reconnaissance. (c) Digital elevation model (DEM) of the area shown in (b) overlain with the mapped ground-surface cracks. m.a.s.l., meters above sea level. The color version of this figure is available only in the electronic edition.

ground-surface displacements were derived. The resultant vectors represent local lateral spread-induced displacements, tectonic movement, and orthorectification/baseline error. The local component of the horizontal movement was isolated by subtracting the average of the horizontal displacements derived for features located outside of the area affected by lateral spreading from the total recorded horizontal displacements in areas where lateral spreading was inferred. The accuracy of the local vectors is approximately ± 0.5 m, which was calculated as the standard deviation of the residuals for local horizontal vectors outside of the area affected by lateral spreading. The accuracy of the methodology was limited by the lack of features identifiable within the greenfield areas proximal to the river in both the pre- and postevent aerial photography. As a

result of the large error ranges, the displacement vectors are used to visually highlight the location and directionality of horizontal ground displacements resulting from lateral spreading and are not used to derive exact displacement values.

Horizontal ground-surface displacements may additionally be derived from comparison of pre- and postevent satellite imagery, as outlined by Martin and Rathje (2014). It is acknowledged that analyses using satellite imagery may result in lower error ranges than those derived from aerial photography; however, it is likely that the use of satellite imagery would also be limited by the lack of identifiable features within the datasets. Analysis of satellite imagery was not undertaken as part of this study due to the lack of readily available data and the time frames required to identify the suite of points required for analysis.

Distributions of Liquefaction Manifestations Following the Kaikōura Earthquake

Distributions Derived from Reconnaissance Mapping

Reconnaissance mapping and visual analysis of postevent aerial photography indicate that localized liquefaction and associated lateral spreading occurred proximal to the Taylor River in central Blenheim and adjacent to Ōpaoa and Lower Wairau Rivers to the east of the township (Fig. 2). The occurrences and spatial extents of liquefaction manifestations are shown to vary along the lengths of the waterways (Fig. 2). Initial comparisons indicate that the distributions were primarily confined to the unprotected floodplain adjacent to the inside banks of meander bends (Fig. 2). Localized cases of liquefaction manifestations were additionally observed in the unprotected floodplain away from meander bends at the Blenheim and Wairau Rowing Clubs and the Marlborough Equestrian Centre (Fig. 2). No damage was recorded in the distal floodplains protected by the stopbank network.

Surface manifestations were generally found to comprise cracking of the ground-surface and localized linear arrays of sand boils orientated subparallel to the closest river bank (Fig. 3). Cracks ranged from greater than 1 m in width proximal to the river banks to a couple of centimeters in width distal to the river banks. The decreasing widths likely reflect decreasing lateral-spread displacements with increasing distance from the river (Fig. 3). Surface sand-blow lineaments composed of gray, poorly graded, and well-sorted fine-to-medium sand were generally observed at distances greater than 20 m from the river banks and ranged from 1 to 2 m in diameter and from 1 to 20 m in length (Fig. 3). Localized stopbank failures were also observed along the Wairau Diversion, Roses Overflow, and at the mouth of the Lower Wairau River (Fig. 3d). Failures generally consisted of cracking along the axis of the stopbank to accommodate ground-surface displacements and exhibited little to no ejecta. Secondary systems of ground cracks and/or sand ejecta were observed at the base of the stopbanks at some sites (Fig. 3d). The observed cracks ranged in width from 0.2 to 0.9 m along the axis of the stopbanks and resulted in an inability of the stopbanks to withhold floodwaters, subsequently requiring emergency remedial works (Fig. 3d).

Field-based reconnaissance mapping enabled liquefaction manifestations to be documented in detail at sites where liquefaction was initially reported and/or observed during drive-by surveys. It is likely that areas of marginal manifestations and/or manifestations in greenfield areas went unreported, due to the time frames associated with the reconnaissance investigations, tendency to focus on areas with severe manifestations, and limitations in accessing private land.

Refining the Spatial Extent of the Areas Affected Using Remote Sensing

Vertical displacements derived from lidar surveys additionally outline areas of ground-surface deformation resulting from the Kaikōura earthquake (Fig. 4). Areas of significant subsidence (> 0.4 m) correspond with the locations of ground-surface cracking mapped from the postevent aerial photography. Subsidence is therefore interpreted to coincide with areas affected by lateral spreading (Fig. 4b). Areas with vertical displacements < 0.2 m are generally positioned outside of the areas with mapped cracks, thus indicating that the aerial photographs and field-based surveys were unable to capture small-scale displacements and deformations. The strong relationship between observed liquefaction manifestations and vertical displacements > 0.2 m indicates that analysis of pre- and postevent lidar may be used to identify distributions and maximum extents of lateral spreading in the absence of ground-based reconnaissance. It may therefore be inferred that the distributions of cracks mapped along the Lower Wairau River closely approximate actual extents and distributions of lateral spreading.

The derived horizontal displacement vectors provide additional information on the direction and magnitude of horizontal ground-surface displacements resulting from lateral spreading (Fig. 4). Horizontal displacements in areas of recorded subsidence are shown to be directed toward the closest river bank and are therefore consistent with the deformation being induced by lateral spreading (Fig. 4a). No inferences can be made on the total horizontal ground-surface displacements in these areas, due to the limited spatial resolution and number of vectors derived. The horizontal displacement vectors, therefore, provide an indication of the severity of lateral spreading and associated ground displacements; however, they do not assist in deriving the maximum inland extent of lateral spreading (Fig. 4a).

The correlation between liquefaction manifestations mapped during reconnaissance investigations and those derived from the lidar and air-photo datasets indicates that remote sensing may be employed to estimate the locations and extents of liquefaction manifestations in areas where ground-based reconnaissance may be limited and/or considered unfeasible.

Sedimentologic and Geomorphological Influences on the Distribution of Liquefaction Manifestations

Detailed mapping through reconnaissance surveys, aerial photography, and lidar survey-derived subsidence indicates that the distribution of liquefaction manifestations varied spatially across the Wairau Plains following the Kaikōura earthquake. Postevent modeling by Bradley *et al.* (2017) indicated that the PGA of 0.22*g* recorded at the MGCS strong-motion station did not exhibit significant spatial variability across the region. It is therefore considered unlikely that spatial variations in the extents of liquefaction manifestations within the Wairau Plains reflect variations in the seismic demand. The mapped extents indicate that liquefaction manifestations were primarily confined to the unprotected floodplains adjacent to inside banks of meander bends of the Ōpaoa and Lower Wairau Rivers in the lower portion of the Wairau Plains (Fig. 2). The observed distributions indicate that a basic understanding of fluvial geomorphology and depositional processes of meandering rivers may be employed to interpret the distribution and sediment types in areas of liquefaction manifestations.

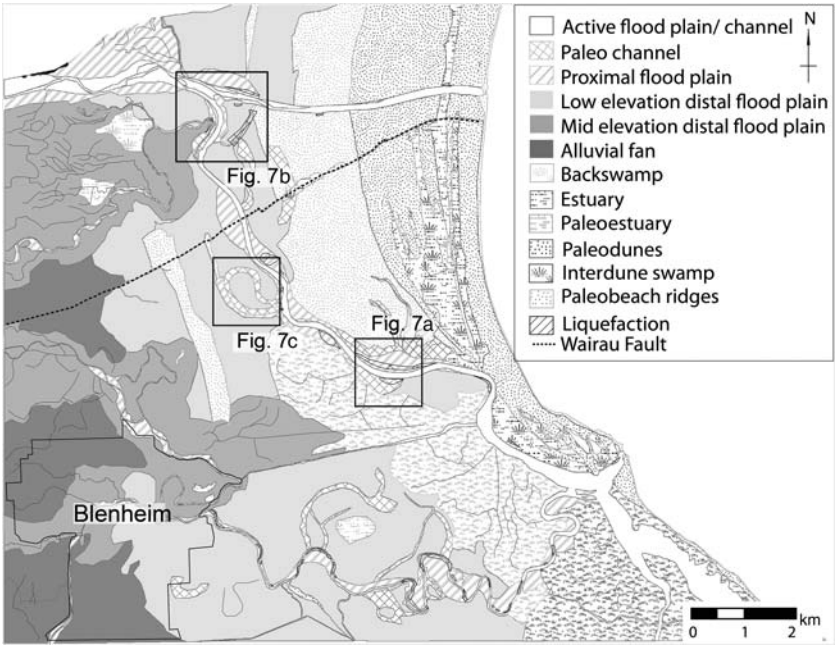

Figure 5. Geomorphic map of the lower portion of the Wairau Plains as mapped from the pre-event DEM overlain with the mapped distribution of liquefaction manifestations following the 2016 Kaikōura earthquake.

The geomorphology of the lower portion of the Wairau Plains was mapped in detail as part of this study from subtle variations in topography observed within the pre-event DEM and is presented in Figure 5. The result was supplemented with analysis of river morphologies, historical maps, and literature outlining drainage modification and the history of the plains (e.g., Cook, 1895; Basher *et al.*, 1995). The pre-event DEM indicating topographic variability across the lower Wairau Plains is presented in Figure 6.

The morphology of the Lower Wairau and Ōpaoa Rivers is typical of meandering rivers and is characterized by a single sinuous channel which forms meander bends. Meandering rivers typically migrate across their alluvial plain as a result of erosion and retreat of the outer banks and subsequent re-deposition on the adjacent inner bank. Erosion occurs as the highest flow velocities are concentrated toward the outer banks during bank-full conditions; the flow is then deflected toward the adjacent inner bank where eroded sediments are deposited. The deposited sediments typically comprise fine sand grading to silt and are termed point-bar deposits. Point-bar deposits may be interbedded with overbank flood deposits that typically comprise fine-to-medium sand to silt (Fryirs and Brierley, 2012). The surrounding alluvial plain typically contains overbank deposits of fine sand to silt deposited as the river overtops its banks during flood events. Swamps generally form distal to the river in areas where standing water remains following flood events (Fryirs and Brierley, 2012). The river channel may rapidly avulse across the alluvial plain in response to a sudden shift in the river course and may cut off a meander bend, forming an oxbow lake. Abandoned river channels, termed paleochannels, may be preserved in the landscape as topographic depressions that are typically infilled with channelized fine-to-medium sands, overlain by silts deposited as flow rates waned (Fryirs and Brierley, 2012). The geologically young, unconsolidated, and saturated nature of the point-bar and paleochannel deposits make them highly susceptible to liquefaction, as illustrated following recent earthquakes (e.g., Wakamatsu, 2012; Wotherspoon *et al.*, 2012). The limited deposition on the outer bank and predominance of silts in the distal floodplain result in lower liquefaction susceptibilities of the underlying sediments.

The observed extents of liquefaction manifestation along the Ōpaoa River are shown to predominantly correspond with the position of point-bar deposits adjacent to the inside banks of meander bends within the proximal floodplain (Fig. 5). Additional areas of observed liquefaction are shown to correspond with the positions of paleochannels of the Lower Wairau River outlined in historical maps (i.e., Cook, 1895). For example, liquefaction manifestations observed at the Blenheim Rowing Club correspond with an area of low topographic relief (0.5–1 m) that is indicated in historical maps as comprising the former S-bend of the Lower Wairau River prior to straightening (Fig. 7a). The affected area is therefore inferred to be underlain by young, unconsolidated, and saturated paleochannel deposits that most likely comprise fine-to-medium sands. In addition, liquefaction manifestations at the

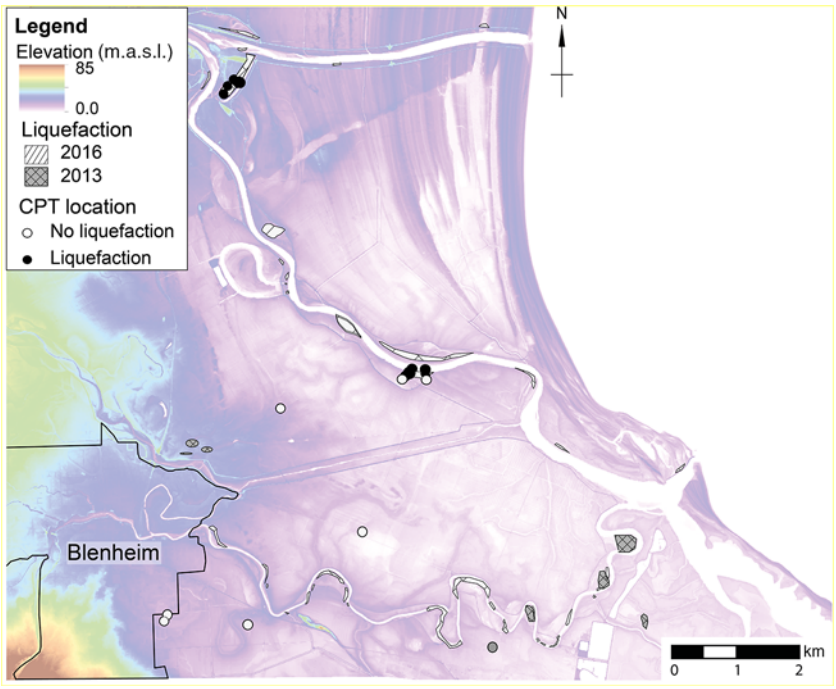

Figure 6. DEM of the lower Wairau Plains with the distribution of liquefaction manifestations mapped following the 2016 Kaikōura and 2013 Lake Grassmere earthquakes indicated. Locations of cone penetration test (CPT) at sites of liquefaction and no-liquefaction manifestation and plotted in Figure 8 are also indicated. The color version of this figure is available only in the electronic edition.

Marlborough Equestrian Park correspond with the position of point-bar and paleochannel deposits associated with a former meander bend of the Lower Wairau River that was diverted during construction of the Wairau Diversion (Fig. 7b). Localized stopbank failures along the adjacent section of the Wairau Diversion additionally correspond with the position of the paleochannel (Fig. 7b).

Liquefaction manifestations observed at the Wairau Rowing Club also correspond with the position of point-bar and paleochannel deposits associated with a former meander bend of the Wairau River (Fig. 7c). The meander bend was cut off from the river during a flood event prior to European settlement, forming Grovetown Lagoon (Fig. 7c).

No liquefaction manifestations were observed within the alluvial plain protected by the stopbank network in the lower portion of the Wairau Plains (Fig. 2). The protected alluvial plain is transected by a series of paleochannels that are recognizable as topographic depressions within the DEM and likely contain loosely consolidated fine-to-medium sands overlain by silt (indicated in Fig. 5).

Prior to the 2016 event, liquefaction was reported following the 2013 Lake Grassmere earthquake (van Dissen *et al.*, 2013). Reconnaissance mapping indicated that the observed liquefaction manifestations were confined to the paleochannels within the distal floodplain (indicated in Fig. 6; van Dissen *et al.*, 2013). It is therefore possible that localized liquefaction manifestations did occur in these paleochannels during the Kaikōura earthquake; however it went unreported due to the rural nature of the area and restrictions in accessing the farmland. The vertical displacement dataset is not able to resolve localized cases of liquefaction, due to limitations in the measurement accuracy and comparably small size of the paleochannels.

In addition, liquefaction manifestations were not observed to the west of the township, which is predominantly underlain by outwash gravels that have been re-worked and re-deposited by the Upper Wairau River and rivers fed from the mountain ranges to the south (Fig. 1). The area is at a higher elevation to the lower portion of the Wairau Plains, resulting in a greater depth to the groundwater table (> 30 m). The depth to groundwater combined with the predominance of gravels, results in a lower liquefaction hazard compared with the east.

Comparison of Subsurface Sediment Profiles in Areas of Liquefaction and No-Liquefaction Manifestation

The observed distributions of liquefaction manifestations following the 2016 Kaikōura earthquake are shown to be confined to the proximal unprotected floodplain adjacent to the meandering Ōpaoa and Wairau Rivers in the lower portion of the Wairau Plains (Fig. 2). The areas of observed manifestation are shown to correspond with areas of low topographic relief that are underlain by point-bar and paleochannel deposits (Fig. 5). Comparison of CPT data from soundings conducted in areas where liquefaction was and was not observed enables variability in the subsurface soil profiles to be examined. The soil behavior type (I_c) is inferred from the relative resistance of the subsurface sediments derived from the CPT and provides an indication of the subsurface stratigraphy. Soils are classified as gravelly-to-dense sand ($I_c < 1.31$), clean sand to silty sand (I_c 1.31–2.05), silty sand to sandy silts (I_c 2.05–2.6), clayey silt to silty clays (I_c 2.6–2.95), silty clay to clay (I_c 2.95–3.6), or peats ($I_c > 3.6$) (Robertson and Wride, 1998). The distribution of CPT soundings in the Wairau Plains is outlined in Figure 6.

CPT soundings conducted in areas where liquefaction manifestations were observed following the 2016 earthquake indicate that the subsurface sediments comprise loose silty sands to sandy silts (I_c 2.05–2.6) that transitions to loose clean sand to silty sand (I_c 1.31–2.05) between 4 and 6 m depth (indicated in Fig. 8a,b). The loose sand to silt likely reflects the geologically young point-bar and paleochannel deposits. In comparison, CPT conducted at sites where liquefaction was not observed following the 2016 earthquake indicates that the subsurface sediments comprise higher

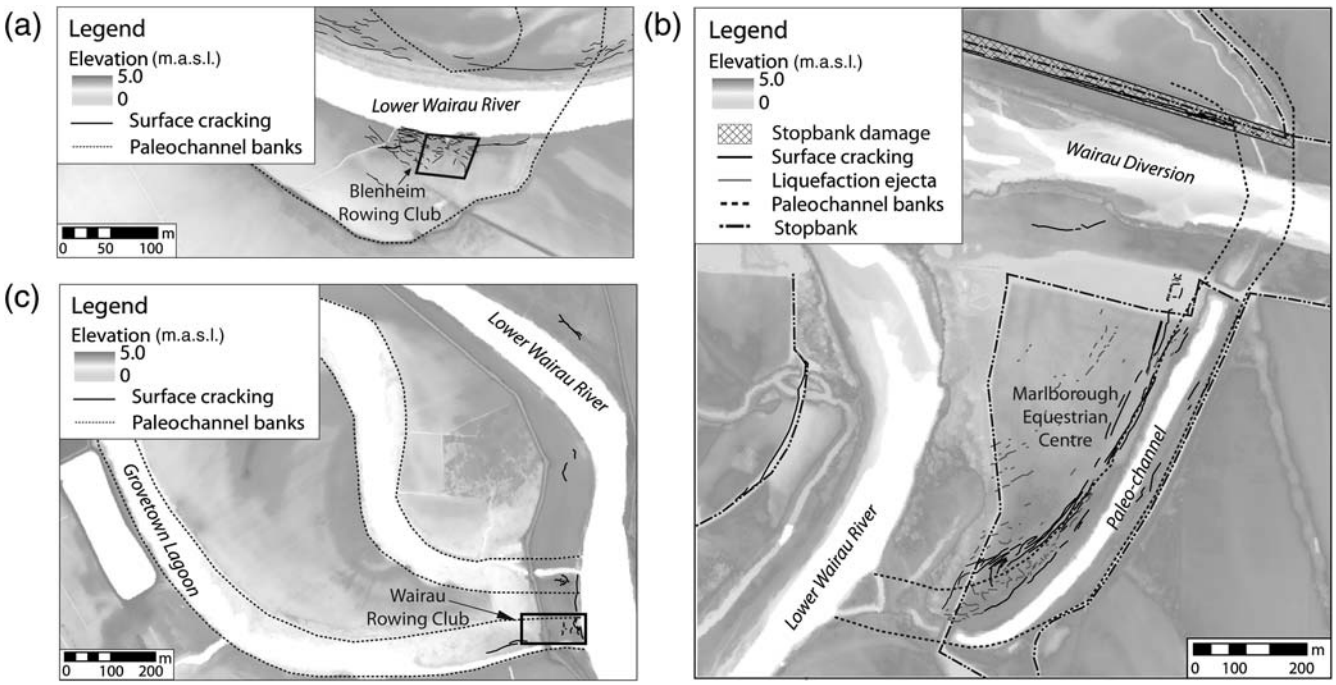

Figure 7. (a) The distribution of liquefaction-induced damage is shown to correspond with the position of the paleochannels of the Lower Wairau River at the Blenheim Rowing Club. (b) The mapped distribution of liquefaction manifestations at the Marlborough Equestrian Centre and stopbank failure along the Wairau diversion are shown to correspond with a paleochannel of the Wairau River cut off during construction of the diversion. (c) Surface cracking at the Wairau Rowing Club also corresponds with the position of paleochannel deposits associated with the cutoff meander bend (Grovetown Lagoon).

density interlayered gravels, silts, and clays (indicated in Fig. 8c,d). These sediments likely reflect older distal floodplain deposits and/or gravel lenses associated with paleochannels of the Wairau River. Further work including additional testing in areas located immediately outside of the area where liquefaction manifestations were observed is required to determine the scale over which the subsurface sediment profiles vary and is the subject of ongoing work.

Implications for Future Liquefaction Potential

The distributions of liquefaction manifestations within the Wairau Plains following the 2016 Kaikōura earthquake are shown to closely correspond with local geomorphic and sedimentologic variability. Liquefaction manifestations are observed within the low elevation point-bar and paleochannel deposits of the meandering Ōpaoa and Lower Wairau Rivers (Fig. 6). Prior to the Kaikōura earthquake, liquefaction manifestations had been reported proximal to the Ōpaoa River and within associated paleochannels following the 2013 M_w 6.5 Lake Grassmere earthquake (indicated in Fig. 6; van Dissen *et al.*, 2013). The comparably more widespread distributions of liquefaction manifestation following the Kaikōura earthquake likely result from the higher PGA and longer duration of shaking compared with the Lake Grassmere earthquake, which generated a local PGA of 0.14*g* (van Dissen *et al.*, 2013). Liquefaction manifestations were additionally reported proximal to rivers and streams within the lower portion of the Wairau Plains following the 1855 M_w 8.2 Wairarapa and 1948 M_w 7.8 Marlborough earthquakes (Mason and Little, 2006). The identification of recurrent liquefaction within the Wairau Plains indicates that the underlying sediments are highly susceptible to liquefaction and that the sediments have remained highly susceptible to liquefaction between events. The direct and consistent correlations between the distributions of liquefaction manifestations and fluvial geomorphology highlight the potential applications of geomorphic mapping, in addition to geotechnical testing, to identify areas underlain by sediments susceptible to liquefaction.

The consistency in the observed distributions of liquefaction manifestations between events suggests that future earthquakes generating similar regional seismic demands would likely result in similar distributions of liquefaction manifestations to those observed following the 2013 and 2016 events. No direct inferences can be made on the likely manifestations resulting from events generating higher PGA nor those resulting from ruptures on local faults. Local fault ruptures would likely generate higher seismic demands, and thus more widespread distribution of liquefaction manifestations may be anticipated.

The observed relationships between fluvial geomorphology and the distribution of liquefaction manifestations within Blenheim following recent and historical earthquakes reiterates the importance of undertaking detailed desktop studies, including collating geomorphic and historical maps, when assessing liquefaction hazards.

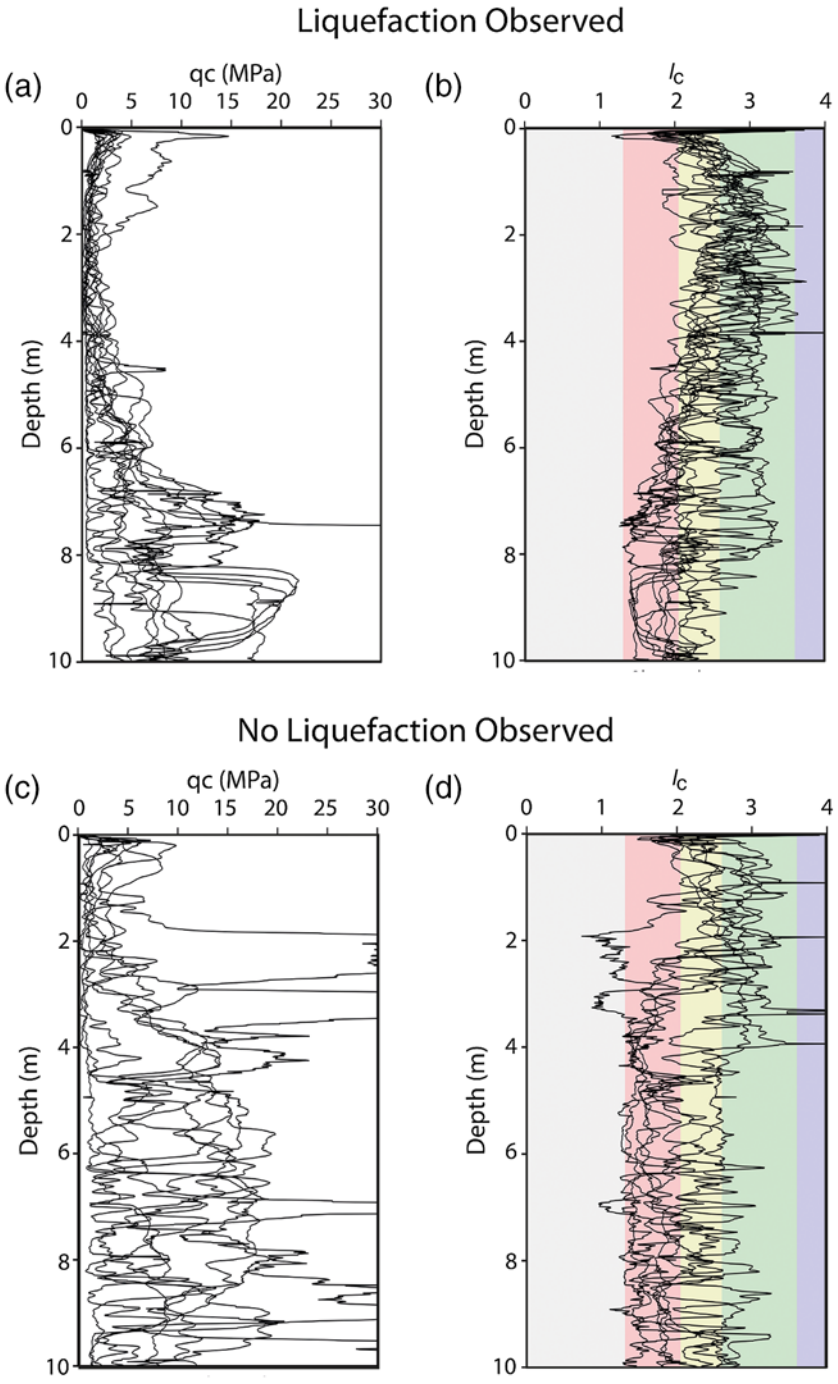

Figure 8. (a) qc (cone tip resistance) logs of CPT conducted in areas where liquefaction manifestations were observed in 2016. The plots indicate loose sediments are present to 7 m depth, at which point the densities increase. (b) I_c (soil behavior type index) logs of the CPT conducted in areas where liquefaction manifestation was reported indicate the sediment predominantly comprises silty sands to sandy silts (I_c 2.05–2.6) that transitions to loose clean sand to silty sand (I_c 1.31–2.05) between 4 and 6 m depth. (c) qc logs of CPT in areas of no reported liquefaction manifestation indicate that the subsurface sediments exhibit higher densities and/or interlayering of dense and less-dense sediments. (d) I_c logs of CPT in areas of no reported liquefaction manifestation indicate that the sediment type exhibits significant variability within the upper 4 m. Sediments below 4 m generally correspond with clean sand to silty sand (I_c 1.31–2.05), silty sand to sandy silts (I_c 2.05–2.6), and exhibit interlayering. The color version of this figure is available only in the electronic edition.

Conclusions

The 2016 Kaikōura earthquake triggered localized liquefaction within the Wairau Plains in the northeast corner of the South Island of New Zealand. Reconnaissance mapping supplemented with postevent aerial photography provided an overview of the liquefaction-induced damage within the region. Vertical ground-surface displacements derived from the comparison of pre- and postevent lidar surveys and horizontal ground displacements inferred from aerial photography enabled the spatial extents of areas affected by liquefaction to be further refined. The derived displacements additionally enabled targeted subsurface geotechnical investigations to be undertaken to better resolve the ground conditions at sites of liquefaction across the Wairau Plains. The observed correlations between mapped liquefaction manifestations and vertical ground deformations derived from lidar indicate that remote sensing may be employed to estimate the locations and extents of liquefaction manifestations in areas where ground-based reconnaissance may be limited and/or considered unfeasible.

Prior to the 2016 Kaikōura earthquake, liquefaction had been reported proximal to rivers and streams within the Wairau Plains following the 1848 Marlborough, 1855 Wairarapa, and 2013 Lake Grassmere earthquakes. Collated reports indicate consistencies in the location and extents of liquefaction manifestations following these events. The occurrence of recent and historical episodes of liquefaction within the Wairau Plains indicates that the sediments have remained highly susceptible to liquefaction. The consistencies in the distributions of liquefaction manifestations between these events confirm that point-bar and paleochannel deposits are highly susceptible to liquefaction. No liquefaction has been reported on the outer banks of the meander bends nor in the distal floodplain following the recent or historical events.

The spatial extents and distribution of liquefaction manifestations closely correspond with the position of point-bar and paleochannel deposits of meandering rivers within the lower portion of the Wairau Plains. The direct correlation between

liquefaction and fluvial geomorphology within the Wairau Plains highlights the importance of incorporating geomorphic and historical maps, in addition to geotechnical testing, to identify areas susceptible to liquefaction. Active point-bar deposits are typically recognizable from the morphology of meandering rivers, whereas paleochannels may be recognized from local topography and historical maps. Comparison of CPT logs indicates that the areas in which liquefaction manifestations were observed are underlain by loose sands and silts, whereas no liquefaction was observed in areas underlain by higher density and interlayered gravels, silts, and clays. The detailed comparisons of the observed distribution of liquefaction manifestation with geomorphic variability and subsurface soil profiles across the Wairau Plains are shown to have assisted the interpretation of the region's liquefaction hazard and the characterization of areas underlain by sediments susceptible to liquefaction.

Data and Resources

Pre-event light detection and ranging (lidar) was flown by NZ Aerial Mapping between 23–28 February 2014 and 3 May 2014 and was downloaded from the Marlborough District Council website (https://www.marlborough.govt.nz/services/maps, last accessed August 2017). Postevent lidar was flown by AAM, Ltd., as commissioned by Land Information New Zealand (LINZ) between November 2016 and January 2017. The data were supplied to the researchers by LINZ as part of the ongoing research efforts and are not yet publicly available. Pre-event aerial photography of the Wairau Plains was downloaded from the LINZ website (https://data.linz.govt.nz/layer/3520-marlborough-02m-rural-aerial-photos-2015-16/, last accessed August 2017). Postevent aerial photography was flown by AAM, Ltd. in November 2016 and was downloaded from the LINZ website (https://data.linz.govt.nz/layer/3529-Kaikōura-earthquake-02m-aerial-photos-2016/, last accessed August 2017). Cone penetration data were obtained from the New Zealand Geotechnical Database (www.nzgd.co.nz, last accessed August 2017). Additional cone penetration test (CPT) soundings obtained as part of a wider research effort were provided by researchers at the University of Auckland, the University of Texas at Austin, and Virginia Tech University and are not yet publically available. Historical maps of the Blenheim area were obtained from the Marlborough District Council website (https://www.marlborough.govt.nz/, last accessed August 2017). Published sources are listed in the References section. Historical distributions of liquefaction were obtained from the published sources listed in the References section.

Acknowledgments

The primary support for the New Zealand members was provided by QuakeCoRE, a New Zealand Tertiary Education Commission-funded Center and the Earthquake Commission (EQC). This is QuakeCoRE publication number 0210. Support for the U.S. Geotechnical Extreme Event Reconnaissance (GEER) Team members was provided by the U.S. National Science Foundation (NSF) as part of the GEER Association activity through CMMI-1300744 and Grant Numbers CMMI-1435494 and CMMI-1724575. The authors thank the Marlborough District Council for providing information on the flood-defense infrastructure in Marlborough.

Any opinions, findings, and conclusions or recommendations expressed in this article are those of the authors and do not necessarily reflect the views of the National Science Foundation, EQC, or the host institutions of the authors.

References

Basher, L. R., I. H. Lynn, and I. E. Whitehouse (1995). *Geomorphology of the Wairau Plains: Implications for Floodplain Management Planning*, Manaaki Whenua Press, Lincoln, Canterbury, New Zealand.

Bradley, B. A., H. N. T Razafindrakoto, and M. A. Nazer (2017). Strong ground motion observations of engineering interest from the 14 November 2016 M_w 7.8 Kaikōura, New Zealand earthquake, *Bull. New Zeal. Soc. Earthq. Eng.* **50,** no. 2, 85–93.

Brown, L. J. (1981). Late Quaternary geology of the Wairau Plain, Marlborough, New Zealand, *New Zeal. J. Geo. Geophys.* **24,** no. 4, 477–490.

Chini, M., M. Albano, M. Saroli, L. Pulvirenti, M. Moro, C. Bignami, E. Falcucci, S. Gori, G. Modoni, N. Pierdicca, *et al.* (2015). Coseismic liquefaction phenomenon analysis by COSMO-SkyMed: 2012 Emilia (Italy) earthquake, *Int. J. Appl. Earth Observ. Geoinform.* **39,** 65–78.

Christensen, K., and C. Doscher (2010). The interaction of river engineering and geomorphology in the Lower Wairau River, Marlborough, New Zealand, *J. Hydrol.* **49,** no. 2, 79–98.

Cook, J. (1895). Map of Cloudy Bay survey district, Produced by J. Cook for the *Department of Lands and Survey*, from the National Library of New Zealand archives, www.natlib.govt.nz (last accessed August 2017).

Fryirs, K., and G. Brierley (2012). *Geomorphic Analysis of River Systems: An Approach to Reading the Landscape*, John Wiley & Sons, Chichester, United Kingdom.

Geotechnical Extreme Event Reconnaissance (GEER) (2017). Geotechnical reconnaissance of the 2016 M_w 7.8 Kaikōura, New Zealand, earthquake, *Version 1: November 8, 2011, Report of the National Science Foundation—Sponsored Geotechnical Extreme Events Reconnaissance (GEER) Team*.

Hughes, M., M. C. Quigley, S. van Ballegooy, B. L. Deam, B. A. Bradley, D. E. Hart, and R. Measures (2015). The sinking city: Earthquakes increase flood hazard in Christchurch, New Zealand, *GSA Today* **25,** no. 3, 4–10.

Marlborough Catchment Board (1959). *Wairau Valley Scheme: Scheme and Economic Reports*, Marlborough Catchment Board, Blenheim, New Zealand.

Martin, J., and E. Rathje (2014). Lateral spread deformations from the 2011 Christchurch, New Zealand earthquake measured from Satellite images and optical image correlation, *Proceedings of the 10th U.S. National Conference on Earthquake Engineering: Frontiers of Earthquake Engineering*, Anchorage, Alaska, 21–25 July.

Mason, D. P. M., and T. A. Little (2006). Refined slip distribution and moment magnitude of the 1848 Marlborough earthquake, Awatere fault, New Zealand, *New Zeal. J. Geol. Geophys.* **49,** 375–382.

Quigley, M., M. Hughes, B. Bradley, S. van Ballegooy, C. Reid, J. Morgenroth, T. Horton, B. Duffy, and J. Pettinga (2016). The 2010–2011 Canterbury earthquake sequence: Environmental effects, seismic triggering thresholds and geologic legacy, *Tectonophysics* **672/673,** 228–274.

Rattenbury, M. S., D. B. Townsend, and M. R. Johnston (Compilers) (2006): *Geology of the Kaikōura Area*, Institute of Geological & Nuclear Sciences 1:250,000 Geological Map 13. 1 sheet + 70 p. GNS Science, Lower Hutt, New Zealand.

Robertson, P., and C. Wride (1998). Evaluating cyclic liquefaction potential using the cone penetration test, *Can. Geotech. J.* **35,** no. 3, 442–459.

Stringer, M. E., S. Bastin, C. R. McGann, C. Cappellaro, M. El Kortbawi, R. McMahon, L. M. Wotherspoon, R. A. Green, J. Aricheta, R. Davis, *et al.* (2017). Geotechnical aspects of the 2016 Kaikōura earthquake on the South Island of New Zealand, *Bull. New Zeal. Soc. Earthq. Eng.* **50,** no. 2, 117–141.

Tonkin and Taylor (2015). Canterbury earthquake sequence: Increased liquefaction vulnerability assessment methodology, *Report Prepared for Earthquake Commission, New Zealand*.

van Dissen, R., M. McSaveney, D. Townsend, G. Hancox, T. A. Little, W. Ries, N. Perrin, G. Archibald, G. Dellow, C. Massey, *et al.* (2013). Landslides and Liquefaction generated by the Cook Strait and Lake Grassmere earthquakes: A reconnaissance report, *Bull. New Zeal. Soc. Earthq. Eng.* **46,** no. 4, 196–200.

Wakamatsu, K. (2012). Recurrence of liquefaction at the same site induced by the 2011 Great East Japan earthquake compared with previous earthquakes, *Proc. of the 15th World Conf. on Earthquake Engineering*, Lisbon, Portugal, 24–28 September, Number 4572.

Wotherspoon, L., M. Pender, and R. Orense (2012). Relationship between observed liquefaction at Kaiapoi following the 2010 Darfield earthquake and former channels of the Waimakariri River, *Eng. Geol.* **125,** no. 27, 45–55.

Department of Civil and Natural Resource Engineering
University of Canterbury
Christchurch 8014
New Zealand
sarah.bastin@canterbury.ac.nz
(S.H.B., M.S.)

Tonkin + Taylor Ltd.
105 Carlton Gore Road, Newmarket
Auckland 1023
New Zealand
(M.O., S.v.)

Department of Civil and Environmental Engineering
The University of Auckland
Private Bag 92019
Auckland 1142
New Zealand
(L.M.W.)

Department of Civil and Environmental Engineering
Virginia Tech
750 Drillfield Drive, MC 0105
Blacksburg, Virginia 24061
(R.A.G.)

Manuscript received 3 September 2017;
Published Online 8 May 2018